JMSCR Vol.||03||Issue||06||Page 6295-6309||June 2015

www.jmscr.igmpublication.org Impact Factor 3.79
ISSN (e)-2347-176x

IGM Publication Journal Of Medical Science And Clinical Research
An Official Publication Of IGM Publication

GPU Based Rician Noise Removal in MR Images Using Fast Gradient Projection Algorithm

Authors
Jayabal Papitha, Bakthavachalam Sharmila, Damodaran Nedumaran
Central Instrumentation and Service Laboratory, University of Madras, Guindy Campus,
Chennai 600 0025, Tamil Nadu, INDIA
Corresponding Author
Damodaran Nedumaran
Emails: *dnmaran@gmail.com*

Abstract
This paper presents a combined Fast Gradient Projection Method with Gabor filter technique for removing the Rician noise present in MR images using general purpose Graphics Processing Units (GPUs) and MATLAB. In this work, the capability of GPUs such as processing tens of thousands of threads in parallel on the array of computing units were utilized to implement the various functions involved in the Rician noise removal algorithms in order to achieve higher computing speed required for real-time implementation. In the proposed method, the Gradient projection filter was employed to denoise and to identify the artifacts in the MR images. For estimating the performance of the proposed method, Rician noise of different levels were added to brain MR images and tested in the proposed algorithm. The results of this study reveal that the proposed method removes the Rician noise without affecting the diagnostic details. This is further supported through visual inspection as well as estimated performance metrics.

Keywords: *Fast gradient projection, Gradient projection, GPU, Gabor filter, MRI, Rician Noise, PSNR*

1. Introduction

Many image processing applications involve complex algorithms which utilize parallel computing platform like graphical processor unit (GPU) due to its high memory bandwidth and high-speed computing capability in implementing the various number-crunching image processing operations[1]. For implementing the algorithms in the GPU, several dedicated software tools are available, which require a thorough understanding of the GPU hardware details and application program concepts in addition to good programming skills. But, MATLAB is a versatile platform for implementing several complex operations very easily using the built-in signal and image processing toolkits. In this work, we implemented fast gradient projection algorithm for the removal of Rician noise present in magnetic resonance (MR) images. Most of the real-time image processing techniques require high complex processing algorithms that can be implemented using parallel computing techniques in GPU platform, since GPU is a single processor with built-in multi-processor blocks that can be used effectively in a parallel fashion in order to execute multiple tasks in real-time than the other processor hardware platforms.

The rest of this paper is organized as follows: In Section 2, we briefly review the functionality and applications of the Graphics Processor Unit. Section 3 presents the basics of the MR Images and the overview of Rician noise present in MR images. The basic and mathematical concepts of Gradient projection method and related algorithms are explained in Section 4. In Section 5, we discuss the basics of Gabor filter and its functional parameters. Section 6 briefly describes the various quality measures and materials employed in this work. The results and the concluding remarks of this study are given in Sections 7 and 8, respectively.

2. Graphics Processor Unit

GPU is a hardware equipped with tremendous computational horsepower and high memory bandwidth, which can bring tremendous improvements in pixel processing, graphics design applications and image operations interms of speed and number crunching operations. It is also called Visual Processing Unit (VPU) of a Graphics Card or Graphics Accelerator. To handle independent graphics blocks and to transfer a section of core memory to the video memory, the GPUs are used in the early computer hardware as well as video display units. But, the modern GPU provides fast and efficient calculation of 3D computer graphics using transistors and supports programmable shaders, over-sampling and very high precision color formats. On the other hand, the General Purpose GPUs (GPGPUs) are the new generation of GPUs that are aiming at handling more general, complex, and intensive processing. With the advancements in GPU, several general and specific applications with high data parallelism can be implemented efficiently, since GPGPU supports parallel data processing using large number of processing units integrated within the GPU. Further, it supports single-instruction multiple-date (SIMD) or single-program multiple-data (SPMD) access as well as arithmetic, loading and interpolations units for data pre-processing in addition to the evaluation units for basic functions. The potentiality of GPUs is well documented and is reviewed here. A multidisplinary group discussed the various issues in parallel computing and its device level applications like GPGPU [2]. The potentiality of GPU in diversified applications like simple image processing simulations and morphological edge detection were demonstrated in terms of flexibility and time efficiency [3].

Din [4] implemented the computationally intensive Haralick features and fractal geometry for efficient classification of medical images by harnessing the power of GPU in optimizing the speed and efficiency of texture and fractal analysis using MATLAB. Aldinucci et al.[5] developed two-phase filter algorithm comprising of an adaptive median filter and a regularization method for removing the salt and pepper noise using fast-flow library of the multi-core GPGPUs that achieves both close-to-ideal speedup and very good wall-clock execution results. Mukherjeet et al.[6] developed 3D computed tomography reconstruction algorithm in CUDA-C and OpenCL using CPU in the GPU platform and compared the performance of the algorithm developed using C in the general purpose CPU platform. Pryor et al.[7] analysed the capabilities and applications of GPU in MATLAB and C/C++ environment using Jacket. Nagest et al.[8] studied the parallel processing capabilities of GPU in a computer vision problem and provided the details of the system level design, memory management and implementation stratergies in CUDA environment. Patel[9] demonstrated the power of GPU for real-time image processing application by processing the polarimetric image data in 30 seconds per frame in MATLAB was reduced to 50 ms in CUDA. Torres and Reyes [10] attempted to improve the speed of HIAT (Hyperspectral Image Analysis Toolbox) of MATLAB by using GPU with Jacket Toolbox of MATLAB and achieved a speedup of 4 to 12 times for various hyperspectral imaging algorithms.

3. Magnetic Resonance Image

The magnetic resonance (MR) data are acquired in the form of complex valued data composed of signal and noise in the K-space. In the formation of an image, the distribution of MR data is transformed from Gaussian to Rician because these data are converted into a magnitude image by taking the square root of the sum of the squares of the real and the imaginary part of the complex data in a pixel-wise manner [11]. These magnitude images have various artifacts due to tangled MRI image formation, such as system delay, angle inhomogeneity, non-centered sampling windows, phase variations, eddy current, pulse timing error, coil impedance changes, etc., that affect the image formation using the complex MR data [12]. As a result, the error between the original image and the processed image induces the Rician noise in magnitude MR image. Signal-to-noise ratio (SNR) decreases and reduces the image contrast when there is an increase in Rician noise [13]. Many research papers have been reported about the origin and removal strategies of Rician noise in MR images. Nowak [14] studied the wavelet-domain filtering to remove Rician noise by taking into account of variations in both the signal and the noise. Aelterman et al. [15] used squared and square root of the magnitude for denoising and combined bias removal in wavelet domain, which increases the contrast and PSNR value of the image.

3.1 Rician noise in MRI

Rice conducted a through discussion on the statistics of random noise and found out that the Rician PDF mainly depends on ths signal-to-noise ratio (SNR) of the signal of interest [16]. Marzetta [17] applied an expectation-maximization (EM) algorithm to SAR images that provide a complete iterative solution to the Rician parameter estimation problem.

The moments of Rician PDF can be expressed using Eq. (1).

$$E(m^{\nu}) = (2\sigma^2)^{\nu/2}\ \Gamma\left(1+\nu/2\right)\ {}_1F_1(-\nu/2;\ 1;-A^2/2\sigma^2) \qquad (1)$$

The odd moments are complex and even moments (i.e., when ν is even) are simple polynomials in Rician distribution. However, the function given in Eq. (1) is explained in terms of modified Bessel functions, which can be derived from the analytical expression for the odd moments [14]. In addition to this, Koay and Basser [18] extracted signal intensity and noise variance from the magnitude MR signal using several correction schemes.

Let the phase image of the MR signal be A, and σ^2 be the variance of each Gaussian noise. The probability distribution $P(a,b;A,\sigma)$ of pixel intensities is given by the Eqs. (2), (3), and (4).

$$P(a,b;A,\sigma) = P(a;A,\sigma)P(b;A,\sigma) \qquad (2)$$

$$P(a;A,\sigma) = \exp\left\{-(a-A)^2/2\sigma^2\right\}/(2\pi\sigma^2)^{1/2} \qquad (3)$$

$$P(b;A,\sigma) = \exp(-b^2/2\sigma^2)\ /\ (2\pi\sigma^2)^{1/2} \qquad (4)$$

It can be derived in terms of the polar coordinates $a = M\cos\theta,\ b = M\sin\theta.$ Further, the Rician distribution is calculated by multiplying $P(a,b;A,\sigma)$ with the Jacobian determinant $M \square \partial(a,b)/\partial(M,\theta)$ and integrating over the angular variable θ as given in Eq. (5).

$$P(M;A,\sigma) = M\ \exp\{-(M^2-A^2)/2\sigma^2\}\ I_o(MA/\sigma^2)/\sigma^2 \qquad (5)$$

where I_o is the zero-order Bessel function [12]. The asymptotic expansion of I_o for large values of its arguments is given in Eq. (6).

$$P(M;A,\sigma) \square\ (M/A)^{1/2}\exp\{-(M-A)^2/2\sigma^2\}/(2\pi\sigma^2)^{1/2},\quad A/\sigma\ \ large \qquad (6)$$

Edelstein et al. [19] measured the SNR using the projection method in an NMR imaging system based on a calibration procedure. They assumed that the measure of the gradient strength is the length of the projection given by Eq. (7).

$$G = 2\pi N_p \Delta f / L\gamma \quad (7)$$

where G is the gradient strength in T/m, γ is the gyromagnetic ratio, and N_p is the number of points in projection. The SNR value is measured by estimating the standard deviation of the points along the projection and averaging the NMR projection amplitude. Thus, the signal and noise depend on the square root of the bandwidth of each pixel and volume of the target, respectively.

4. Gradient Projection Method

Bound constrained optimization problems are solved using Gradient Projection (GP) methods. In non-linear programming when constraint functions are linear GP methods are applied. GP method was first introduced by Goldstein [20] and Lewtin & Polyak [21] for resolving convexly constrained minimization problems and regarded as an extension of the steepest descent or Cauchy algorithm for solving unconstrained optimization problems. The search is made along the resulting curve obtained from boundary region obtained by projecting the negative Gradient. In the solution of bound constrained optimization problems, the drawback of the active set methods is that the working set changes slowly; at the most one constraint is added, to or dropped from the working set at each iteration. At each iteration, the gradient-projection algorithm (GPA), the prototypical method, permits large changes in the working set. Upon correct implementation, GPA identifies the active set at a solution in a finite number of iterations. After the identification of the correct active set, the GPA reduces the steepest-descent algorithm on the subspace of free variables. As a result, this method is invariably used in conjunction with other methods for faster rates of convergence [22]. The first results towards the conditions which guarantees GP method identifies the optimal active set in a finite no. of iterations for bound constrained problem was obtained by Bertsekas [23]. Later in 1982, Bertsekas derived some results for a projected Newton Method [24] and Gafini and Bertsekas for a 2-metric projection method [25]. A statement stating that if a strict complementary condition holds, then the GPA identifies the optimal active constraints in a finite no. of iterations was proved by Dunn [26]. The above statement was extended by Burke and More, particularly they proves that under Dunn's non-degeneracy assumption the optimal active constraints are eventually identified if and only if the projected gradient converges to 0 [27]. The converging properties of GP were studied by Calamai and More, and the results were applied for linearly constrained problems [28]. Basically in infinite-dimensional Hilbert spaces GPA has weak Convergence, so an operator oriented averaged mapping approach for providing strong convergence for GPA was provided by Hong-Kun xu [29]. Based on the penalty function approach and GPA, Luenberger proposed a new programming algorithm for non-linear constrained optimization [30]. For a class of stochastic optimal control problems, a simple and effective GPA was stated by Ning Du et al. and its convergence properties were also discussed with extensive numerical tests [31]. A new solution for Side–Constrained Traffic Assignment Problem (SCTAP) was solved using a combination method based on the inner penalty function and path-based adaptation of the GPA [32]. A method for solving quadratic programming reformulation of a class of convex non smooth unconstrained optimization problems using GPA was experimentally elaborated by Fiegueiredo and Nowak in [33]. In [34] Farag investigated the convergence of the GPA by solving some optimal control problems of parabolic equations. For problems having starting guess far from the solution, a piece-wise smooth projection method associated with constrained set defined by bounds on variables and a single linear equation was evaluated by Hager and Park [35].

The Armijo rule along the projection arc and its convergence behavior was studied by Bertsekes [36]. Chambolle made a key breakthrough by proposing a fixed point algorithm and a gradient projection method with constant step size based on the dual formulation of total variation [37,38]. In addition to the above Gradient Projection method is also used for handling image restoration problem like Graph cut methods [38] and the Split Bregman Method [20].

4.1 Algorithm for Gradient Projection:

Considering the problem for minimizing continuously differentiable mapping $f:\mathbb{R}^n \to \mathbb{R}$ on C, a nonempty closed convex set of $\mathbb{R}^n$, the constrained minimization problem is described as equation (8).

$$\min_{x \in C} f(x) \tag{8}$$

where the object function $f(x)$ is a composite type convex function denoted by equation (9)

$$f(x) = F(x) + G(x) \tag{9}$$

In (9) $F(x)$ is the smooth convex function and $G(x)$ is the continuous non-smooth convex function. To solve the minimization problem given in Eq. (8), the GP algorithm is used. It generates a sequence of $\{x_k\}$ through the recursion as in Eq. (10).

$$x_{k+1} = P_c(x_k - \alpha_{k+1}\nabla f(x_k)),\ k+1 \in \mathbb{N}. \tag{10}$$

In Eq. (10) the initial guess is chosen arbitrarily as $x^0 \in C$ and α_k is a sequence of step sizes with $\alpha_{k+1} \geq 0$ for each $k \geq 0$. P_c is the orthogonal projection operator on the set C [39]. By applying a special case of backward-forward splitting method [40], the basic Gradient-based model can be written as Eq. (11):

$$x_{k+1} = \arg\min_x \{G(x) + (1/2\alpha_{k+1})\|x - (x_k - \alpha_{k+1}\nabla f(x_k))\|^2\} \tag{11}$$

The discrete penalized version of the TV based de-blurring model consists of solving an unconstrained convex minimization problem of the form stated in Eq. (12).

$$\min_x \|x-b\|_F^2 + 2\lambda|x|_{TV} \tag{12}$$

where b is the observed noisy data. x is the desired unknown image to be recovered and λ is the regularization parameter with $\lambda > 0$.

Let us consider $C = B_{l,u}$, then $P_c = P_{B_{l,u}}$. Thus GPA can be described in a matrix form as shown in Eq. (13).

$$P_{B_{l,u}}(x)_{ij} = \begin{cases} l & x_{ij} < l \\ x_{ij} & l \leq x_{ij} \leq u \\ u & x_{ij} > u \end{cases} \tag{13}$$

where l is the vector of lower bounds, u is the vector of upper bounds. If $(p,q) \in P$, then the optimal solution of the dual problem with TV based de-noising is given by

$$\min_{(p,q)\in P} \{h(p,q) \equiv -\|H_c(b - \lambda \Omega(p,q)\|_F^2 + \|b - \lambda \Omega(p,q)\|_F^2\} \tag{14}$$

Here $$H_c = x - P_c(x) \text{ for every } x \in \mathbb{R}^{m*n} \tag{15}$$

When TV=TV_1, the solution of Eq. (14) is given by

$$x = P_c(b - \lambda \Omega(p,q)) \tag{16}$$

The objective function h of Eq. (14) is continuously differentiable and its gradient is given by

$$\nabla h(p,q) = -2\lambda \Omega^T P_c(b - \lambda \Omega(p,q)) \tag{17}$$

$$(p_{k+1}, q_{k+1}) = P_p[(p_k, q_k) + (1/8\lambda)\Omega^T(P_c[b - \lambda \Omega(p_k, q_k)])] \tag{18}$$

The optimal solution of the Eq. (14) is given as x^*

$$x^* = P_c[b - \lambda \nabla(p_k, q_k)] \tag{19}$$

where P_p is the projection operator which maps a matrix pair (p,q) with another matrix pair $(r,s) = P_p(p,q)$ and can be readily implemented [41].

4.2 Algorithm for Fast Gradient Projection

For a better rate of convergence, the Fast Gradient Projection (FGP) method is used on the dual problem stated in Eq. (14). Considering, $(r_1, s_1) = (p_0, q_0)$ at step 0, and $k \in$ at step k, the Eq. (14) can be denoted as Eq. (20, 21).

$$(p_{k+1}, q_{k+1}) = P_p[(r_{k+1}, s_{k+1}) + (1/8\lambda) \nabla^T (P_c[b - \lambda \nabla(r_{k+1}, s_{k+1})])] \tag{20}$$

$$\alpha_{k+2} = \{1 + \sqrt{1 + 4\alpha_{k+1}^2}\}/2 \tag{21}$$

$$(r_{k+2}, s_{k+2}) = (p_{k+1}, q_{k+1}) + [(\alpha_{k+1} - 1)/\alpha_{k+2}](p_{k+1} - p_k, q_{k+1} - q_k) \tag{22}$$

5. Total Variation Method

Total variation (TV) is an efficient algorithm for regularizing the images without smoothing the boundaries of the objects. TV was originally developed by Rudin, Osher and Fatemi (ROF) for solving inverse problems in intensity images, later it was extended to color images by Blomgren and Chan [42]. The key idea behind this method is that the integral of the absolute Gradient of the image is high when it has unwanted noise. Basically, the TV of an image gives the change between the pixel values of the image [43]. Let the image acquisition system have the formation as given in Eq. (23).

$$z = (h * v) + n \tag{23}$$

In Eq. (23), v denotes the ideal undistorted image, h is the blurring kernel introduced to restore blurred and noisy image and z is the observed image. n, is the additive Guassian noise with standard deviation σ. Rudin-Osher-Fatemi [44] proposed a solution for solving the constrained minimization problem stated in Eq. (24).

$$\begin{aligned} &\min \int_{\Omega} |Dv| \\ &s.t \int_{\Omega} |h * v(x) - z(x)^2| dx \le \sigma^2 |\Omega| \end{aligned} \tag{24}$$

The problem of de-noising an image contains the case where $h = \delta$, so the Eq. (23) is written as $z = u + n$. Thus the unconstrained variational formulation with above condition is given as Eq. (25). The variation of the additive Guassian white noise of zero mean and variance is σ^2 [45].

$$\min_u \{E(v)\} = \int_{\Omega} |\nabla v(x,y)| d\Omega + (1/2\lambda) \int_{\Omega} |z - v| d\Omega \tag{25}$$

The TV is obtained using the gradient-descent method.

$$\partial v / \partial t = [(v_{xx} v_y^2 - v_x v_y v_{xy} + v_{yy} v_x^2)/(v_x^2 + v_y^2)^{3/2}] - 2\lambda x(v - v_0) \tag{26}$$

In the TV method, the minimized energy functional measures the variation in the image.

6. Gabor Filter

A Gabor filter [47,48] is a multi-resolution filter having responses similar to those of the human visual cortex [46]. Some Gabor filter applications in MR Images were studied in [49-51]. A Gabor filter can be viewed as a sinusoidal plane of particular frequency and orientation, modulated by a Gaussian envelope [52]. The filter can be represented in a complex form as in Eq. (27)

$$g(u,v,\lambda,\theta,\psi,\sigma,\gamma) = \exp[-(u'^2+\gamma^2 v'^2)/2\sigma^2]\exp\{i(2\pi(u'/\lambda)+\psi)\} \quad (27)$$

where $u' = u\cos\theta + v\sin\theta$ and $v' = -u\sin\theta + v\cos\theta$. The wavelength of the sinusoidal factor is represented by λ, the orientation of normal to parallel strips is θ. ψ is the phase off-set and σ, γ represent the sigma of Gaussian envelope and spatial aspect ratio respectively. For efficient noise removal in MR images, the parameters $\theta, \lambda, \psi, \gamma$ and σ of Gabor filter have been assigned to be some optimum values. The orientation angle $\theta \in [0, 2\pi]$. In our work we have chosen $\sigma = 0.25$, $\gamma = 0.5$, $\psi \in (0, \pi/2)$, $\lambda = 1$ and $\theta = 0$.

7. Tools and Data

The filtering algorithms were developed in MATLAB 2011b installed in an Intel® Xeon ® W3565 @ 3.19 GHz processor PC with Windows 7 professional operating system (Model–HP Z400 Workstation). All the algorithms developed are tested on various MR images obtained in the DICOM file format. The details of GPUs and MR brain images are given in Table 1.

Table 1. Detailed specifications of the GPU and the MR brain images used in this study

Specifications of GPU		Specifications of MR image	
Package	parallel.gpu	Scan option	PFP/SART1
Name	'Quadro 600'	MR Acquisition type	3D
Index	1	Reception time	24 ms
Compute capability	2.1	Echo time	7 ms
Supports double	1	Imaging frequency	63.6777 MHz
Driver version	5.5000	Field of view	175×220
Max Grid Size	[65535 65535]	Magnetic field intensity	0.15 T
SIMD Width	32	Image format	DICOM
Total Memory	1.0737e+009	Manufacturer	Siemens Esaote ARTO scan C
Multiprocessor Count	2		

8. Results and Discussions

The algorithm was tested on more than 100 MR images. To study the performance of the filters in removing the Rician noise, two different MR images (the raw MR image (RNoisy) with the actual Rician noise present and the raw MR image 0126049D added with Rician noise of 0.1 and 0.15 levels) were tested on the filtering algorithms, viz., Gradient projection combined with Gabor filter (G+GP), Fast Gradient projection combined with Gabor filter (G+FGP), Total variation filter (TV1) and Total variation filter with two iterations (TV2). Further, the performance of the filters was studied by estimating the quality metrics such as PSNR, MSSIM, CNR, NAE (Normalized Absolute Error), NCC (Normalized Cross Correlation), IQI

(Image Quality Index), and VOI (Variation of Information) of the raw and Rician noise added and their corresponding filtered images.

The MR image (RNoisy) with inherent Rician noise present during acquisition of the image from the equipment and their corresponding filtered images are shown in Fig. 1. The raw MR image 0126049D added with two different levels (0.1 and 0.15) of Rician noise and its corresponding filtered images are given in Figs. 3 and 5. The quality metrics, estimated for all these images are given in Tables 2, 3 and 4. and their respective histogram charts are given in the Figs. 2, 4 and 6, respectively.

From the visual inspection of the MR images by the trained radiologists and the estimated quality metrics arrived out of this study, the following inferences are summarized.

1. The PSNR values estimated from the results of the Gabor with Fast Gradient projection (G+FGP) algorithm exhibit higher values than the other filtering methods, which clearly indicates that the Rician noise is removed effectively.
2. The MSSIM value of the proposed G+FGP method was found to be less, which showed that the G+FGP method reduces the noise structure appreciably, while maintaining the homogeneity of the image intact.
3. The CNR value of the proposed G+FGP filtering method is found to be higher, that exhibits the improvements in the contrast of the image while reduceing the noise.
4. Similarly, the variation of information (VOI) of the proposed G+FGP method is found to be higher due to efficient reduction of noise information.
5. The visual inspection of the images by the trained radiologists conforms that the G+FGP method exhibits better smoothing, more homogeneity, and contrast improvements over the other filtering methods.
6. The GPUs having compute capability (CC) above 1.3 only can perform external programs. Therefore, the proposed algorithm can easily be utilized the benefits of GPGPU (QUADRO 600, CC- 2.1) with very little change in their MATLAB code that accelerates the programs execution speed.

As a result, from the quality metrics and the visual inspection of the filtered images, it is concluded that the G+FGP is the efficient and optimum method in reducing the Rician noise over the G+GP and total variance (TV1 and TV2) methods. Hence the G+FGP method is suggested as the best choice for removing the Rician noise in MR images.

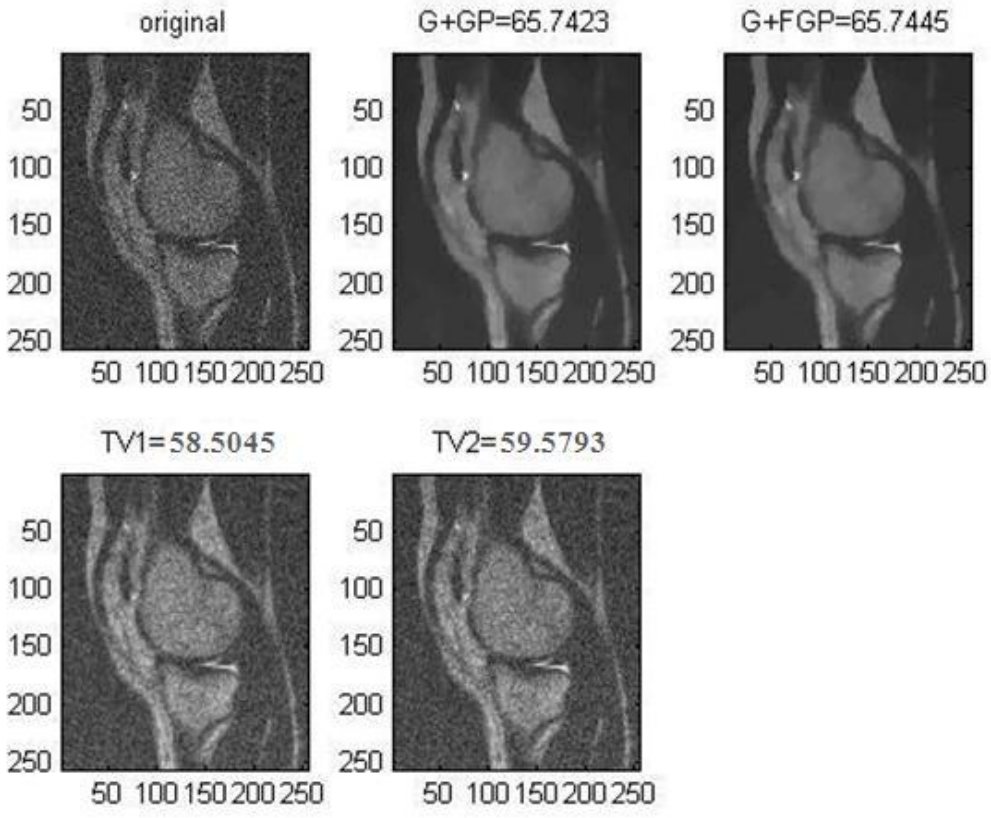

Fig. 1. Raw and filtered RNoisy MR images

Table 2. Estimated Quality Metrics for MR image of RNoisy

Filters / Parameters	G+GP	G+FGP	TV1	TV2
PSNR	65.7423	65.7445	58.5045	59.5793
MSE	0.0173	0.0173	9.1756e-004	7.1639e-004
NAE	0.3818	0.3818	0.1042	0.0890
NCC	0.6227	0.6227	1.0118	1.0109
IQI	0.2215	0.2265	0.7188	0.7962
VOI	0.0850	0.0861	0.0080	0.0080
MSSI	0.9976	0.9976	1.0000	1.0000
CNR	11.2045	11.1976	0.1306	0.1055

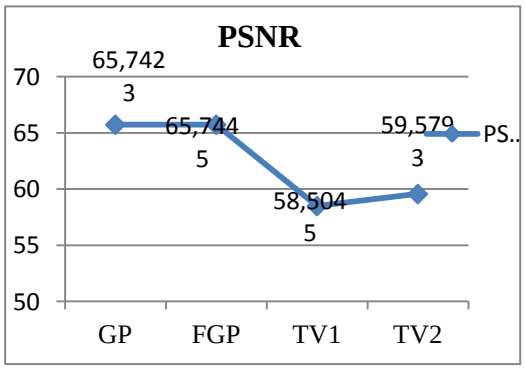

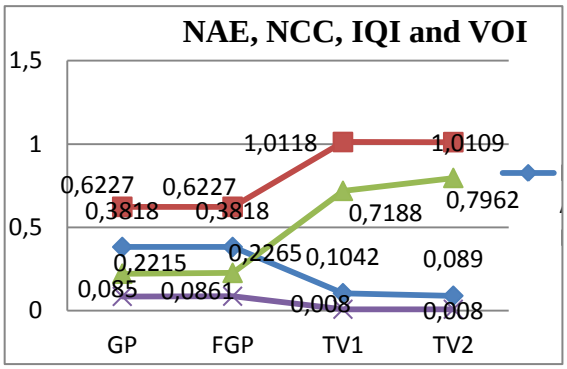

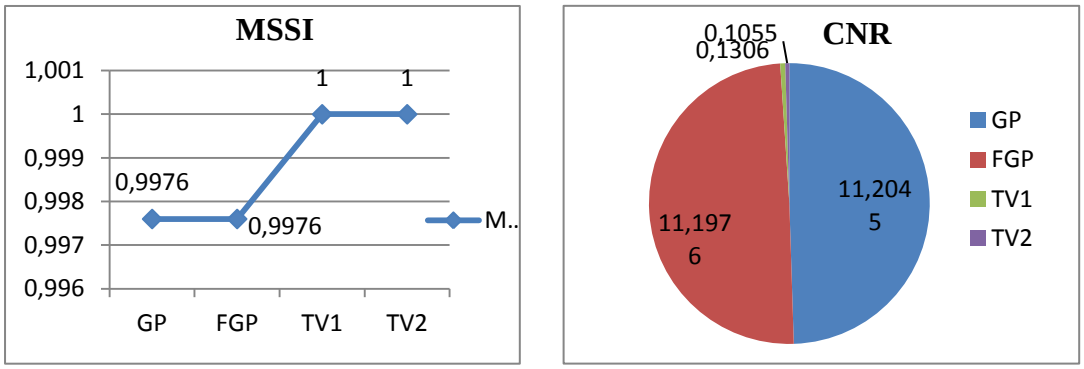

Fig. 2. Histogram plots of the different quality metrics calculated from the filtered RNoisy MR image

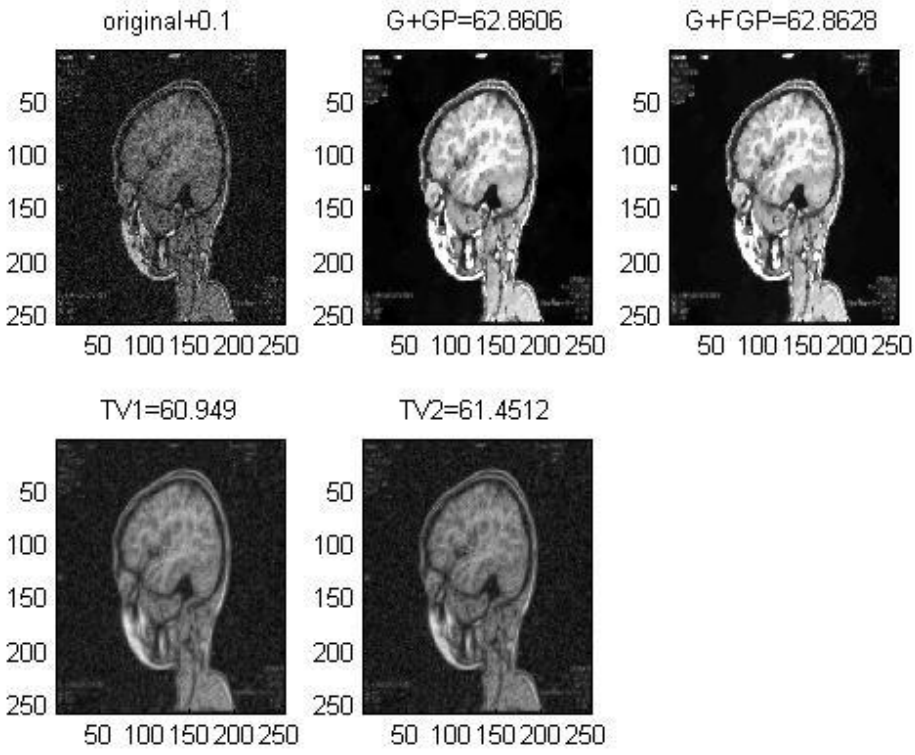

Fig. 3. Raw MR image (0126049D) corrupted with Rician noise level of 0.1 and its corresponding filtered images

Table 3. Estimated Quality metrics of MR image (0126049D) corrupted with Rician noise level 0.1

Filters / Parameters	G+GP	G+FGP	TV1	TV2
PSNR	62.8606	62.8628	60.9490	61.4512
MSE	0.0337	0.0336	0.0523	0.0466
NAE	0.3887	0.3886	0.5198	0.4440
NCC	0.6450	0.6450	0.7693	0.7921
IQI	0.3440	0.3450	0.6542	0.6802
VOI	0.8731	0.8727	0.6464	0.6104
MSSI	0.9958	0.9958	0.9969	0.9974
CNR	1.4143	1.4149	0.1430	0.1198

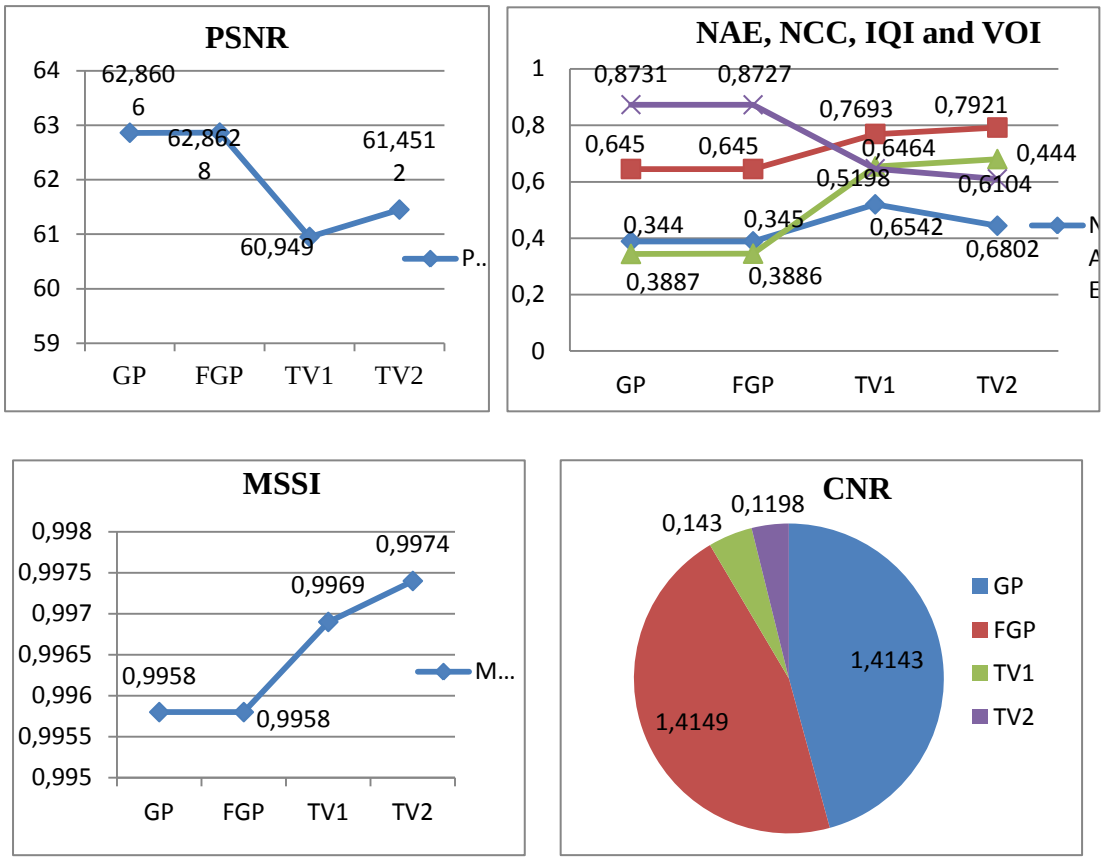

Fig. 4. Histogram plots of the estimated quality metrics of the MR image (0126049D) corrupted with Rician noise level 0.1

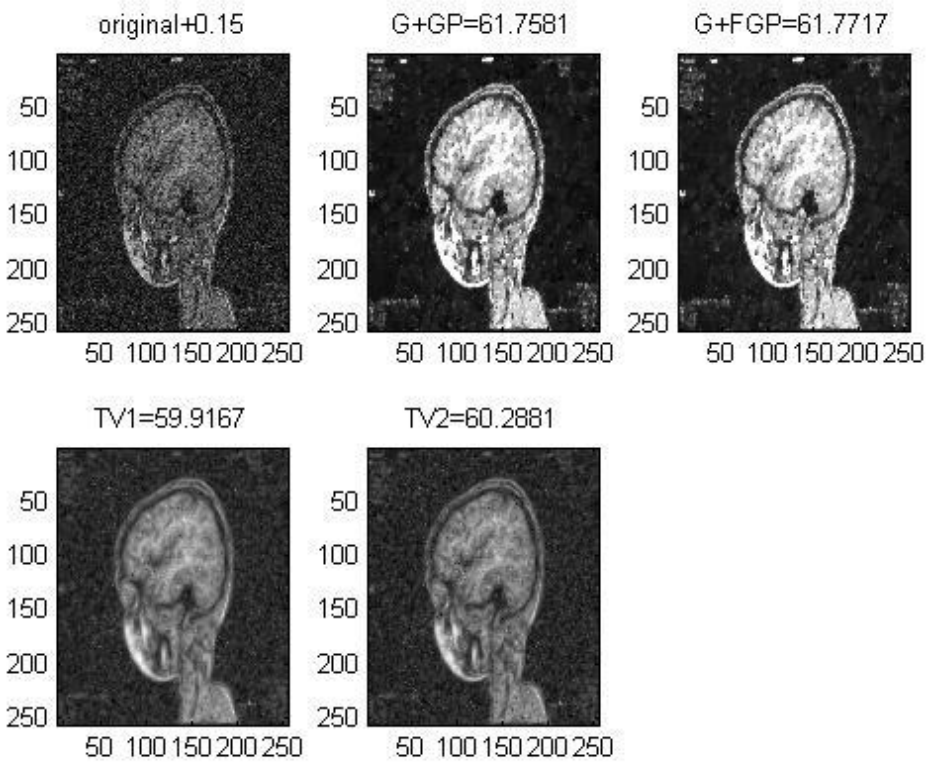

Fig. 5. Raw MR image (0126049D) corrupted with Rician noise level of 0.15 and its corresponding filtered images

Table 4. Estimated Quality metrics of MR image (0126049D) corrupted with Rician noise level 0.15

Filters / Parameters	G+GP	G+FGP	TV1	TV2
PSNR	61.7581	61.7717	59.9167	60.2881
MSE	0.0434	0.0432	0.0663	0.0609
NAE	0.3867	0.3863	0.5897	0.5218
NCC	0.6478	0.6481	0.7448	0.7644
IQI	0.4248	0.4301	0.4934	0.5179
VOI	0.9246	0.9212	0.7616	0.7326
MSSI	0.9948	0.9948	0.9960	0.9966
CNR	1.9258	1.9295	0.1654	0.1448

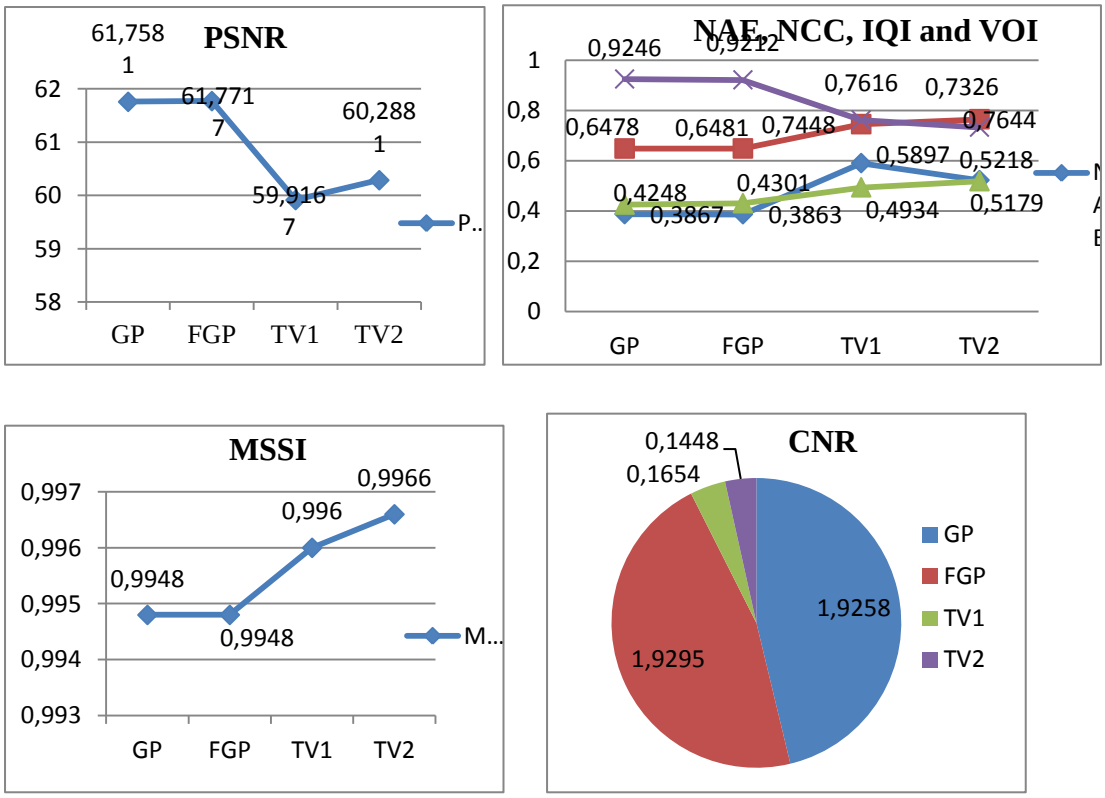

Fig. 6. Histogram plots of the estimated quality metrics of the MR image (0126049D) corrupted with Rician noise level 0.15

9. Conclusion

In this work, we implemented the Gabor filter combined with the Fast Gradient Projection filter (G+FGP) technique developed in MATLAB for removing the Rician noise present in MRI images in the General Purpose Graphics processor environment. The performance of the developed method was estimated qualitatively as well as by visual inspection. The results showed that the G+FGP removes the signal dependent bias effectively, which is evident from the increase in peak signal to noise ratio values. Also, the G+FGP method improved the contrast of the image, which is very much useful in the diagnosis of tissue characterization. In the future scope of this study, all these techniques will be implemented in the GPUs with a parallel processing algorithm for an efficient time reducing process.

Acknowledgment

JP would like to thank the University of Madras for the award of a University Research Fellowship. BS is grateful to the Department of Science and Technology (DST) for financial assistance through an INSPIRE fellowship.

References

1. Kong J, Dimitrov M, Yang y, Liyanage J, Cao L, Staples J, Mantor M, Zhou H. Accelerating MATLAB Image Processing Toolbox Functions on GPUs. The 3rd workshop on General-Purpose Computation on Graphics Processing Units (GPGPU-3) 2010; pp. 75–85.
2. Asanovic K, Bodik R, Catanzaro B, Gebis J, Husbands P, Keutzer K, Patterson D, Plishker W, Shalf J, Williams S, Yelick K. The landscape of parallel computing research: A view From Berkeley. Tech. Rep. No. UCB/EECS-2006-183 2006; p. 54 .
3. Marwa C, Fatma S, Rached T. Computer Vision Application in Graphic Processors. Laboratory of Electronics and Microelectronics. The 2012 International Conference on Image Processing, Computer Vision, and Pattern Recognition (IPCV'12) 2012.
4. Din R. Matlab Medical Images Classification On Graphics Processors. U.P.B. Sci. Bull. Series C 2013; p. 75, ISSN 2286-3540.
5. Aldinucci M, Spampinato C, Drocco M, Torquati M, Palazzo S. A Parallel Edge Preserving Algorithm for Salt and Pepper Image Denoising. 3rd International Conference on Image processing theory, tools and applications (IPTA) 2012; pp. 97–104, 10.1109/IPTA.2012.6469567.
6. Mukherjeet S, Moore N, Brock J, Leeser M. CUDA and OpenCL implementations of 3D CT reconstruction for biomedical imaging. IEEE Conference on High Performance Extreme Computing (HPEC) 2012; pp. 1–6, DOI.10.1109/HPEC.2012.6408674.
7. Pryor G, Lucey B, Maddiapatla S, McClanahan C, Melanokos J, Venugopalakrishnan V, Patel K, Yalamanchilli P, Malcolm J. High-level GPU computing with jacket for MATLAB and C/C++. Modelling and Simulation for Defense Systems and Applications VI 2011; DOI. 10.1117/12.884899.
8. Nagesh P, Gowda R, Li B. Fast GPU implementation of large scale dictionary and sparse representation based vision problems. IEEE International Conference on Acoustics Speech and Signal Processing (ICASSP) 2010; pp. 1570–1573, DOI. 10.1109/ICASSP.2010.5495526.
9. Patel H. GPU accelerated real time polarimetric image processing through the use of CUDA. IEEE Proc. of Aerospace and Electronics Conference (NAECON) 2010; pp. 177-180, DOI.10.1109/NAECON.2010.5712943.
10. Torres RS, Reyes VM. Speeding up the MATLAB™Hyperspectral Image Analysis Toolbox using GPUs and the Jacket Toolbox. Hyperspectral Image and Signal Processing: Evolution in Remote Sensing. WHISPERS'09 2009; pp. 1–4, DOI. 10.1109/WHISPERS.2009.5289089.
11. Sijbers J, Dekker AJ. Maximum likelihood estimation of signal amplitude and noise variance from MR data. Magn. Reson. Med 2004; 51(3): 586–594.
12. Bernstein MA, Thomasson DM, Perman WH. Improved detectability in low signal-to-noise ratio magnetic resonance images by means of a phase-corrected real reconstruction. Med. Phys 1989; 15(5): 813–817.
13. Landini L, Positano V, Santarelli MF. Advanced Image Processing in Magnetic Resonance Imaging. Taylor & Francis Group. LLC 2005; ISBN-10: 0-8247-2542-5.
14. Nowak RD. Wavelet-based Rician noise removal for magnetic resonance images. IEEE Transaction on Image Processing 1999;10(8): 1408–1419.

15. Aelterman J, Goossens B, Pizurica A, Philips W. Removal of Correlated Rician Noise in Magnetic Resonance Imaging. 16th European Signal Processing Conference (EUSIPCO 2008) Switzerland 2008; pp. 25–29.
16. Rice SO. Mathematical Analysis of Random Noise, Bell System Technical Journal 1944; 23(24): 282–332.
17. Marzetta TL. EM algorithm for estimating the parameters of a multivariate complex Rician density for polarimetric SAR. IEEE Conference proceedings in Acoustics, Speech, and Signal Processing 1995.
18. Koay CG, Basser PJ. Analytically exact correction scheme for signal extraction from noisy magnitude MR signals. J. of Magn. Reson. 2006; 179(2): 317–322.
19. Edelstein WA, Bottomley PA, Pfeifer LM. A signal-to-noise calibration procedure for NMR imaging systems. Med. Phys 1984; 11(2): 180–185.
20. Goldstein AA. Convex programming in Hilbert space. Bull. Amer. Math. Soc. 1964; 70: 709–710.
21. Levitin ES, Polyak BT. Constrained minimization problems. U.S.S.R. Comput. Math. Math. Phys. 1966; 6(5): 1–50.
22. Bertsekas DP. Nonlinear programming. Athenas Scientific 1995; pp. 22-75 and 223-272. ISBN**:** 1-886529-00-0.
23. Bertsekas DP. On the Goldstein - Levitin - Polyak Gradient Projection Method. IEEE Transactions on Automatic Control 1976; 21(2): 174–184.
24. Bertsekas DP. Projected Newton methods for optimization problems with simple constraints. SIAM J. Control and Optimization 1982; 20(2): 221–246.
25. Gafni EM, Bertsekas DP. Convergence of a Gradient Projection Method. Massachusetts Institute of Technology. Laboratory for Information and Decision Systems 1982; pp. 1–12.
26. Dunn JC. On the convergence of projected gradient processes to singular critical points. J. Optim. Theory. Appl. 1987; 55(2): 203–216. DOI 10.1007/BF00939081.
27. Burke JV, More JJ. On the identification of active constraints. SIAM J. Numer. Anal. 1988; 25(5): 1197–1211.
28. Calamai PH, More JJ. Projected Gradient Methods for linearly constrained problems. Mathematical Programming. Springer-Verlag New York 1987; 39(1): 93–116.
29. Xu HK. Averaged Mappings and the Gradient-Projection Algorithm. J. Optim. Theory. Appl. Springer 2011; 150: 360–378. DOI 10.1007/s10957-011-9837-z.
30. Luenberger DG. A Combined penalty function and gradient projection method for nonlinear programming. J. Optim. Theory. App. 1974; 14(5): 477–495.
31. Du N, Shi J, Liu W. An effective gradient projection method for stochastic optimal control. Int. J. Numer. Anal. Model. 2013; 10(4): 757–774.
32. Prashker JN, Toledo T. A Gradient Projection algorithm for side-constrained traffic assignment. Eur. J. Transp. Infrast. 2004; 4(2): 177–193.
33. Figueiredo AT, Nowak RD. Gradient projection for sparse reconstruction: application to compressed sensing and other inverse problems. IEEE J. Sel. Top. Sign. Proces. 2007; 1(4): 586–597.
34. Farag MH. The Gradient Projection method for solving an optimal control problem. Applicationes Mathematicae 1996; 24(2): 141–147.
35. Hager WW, Park S. The Gradient Projection method with exact line search. J. Global. Optim. 2004; 30: 103–118.
36. Chen P, Gui C. " Linear convergence analysis of the use of gradient projection methods on the total variation problems. Comput. Optim. Appl. 2013; 54(2): 283–315.

37. Chambolle A. An Algorithm for total variation minimization and applications. J. Math. Imaging. Vis. 2004; 20: 89–97.
38. Chambolle A. Total Variation Minimization and a Class of Binary MRF Models. Energy minimization methods in computer vision and pattern recognition. Springer. 5th International Workshop, EMMCVPR Proceedings 2005; 3757: 136–152. DOI 10.1007/11585978_10.
39. Beck A, Teboulle M. Fast gradient-based algorithms for constrained total variation image denoising and deblurring problems. IEEE Transactions on Image Processing 2009; 18(11): 2419–2434. DOI 10.1109/TIP.2009.2028250.
40. Passty GB. Ergodic Convergence to a Zero of the Sum of Monotone Operators in Hilbert Space. J. Math. Anal. Appl. 1979; 72: 383–390.
41. Soman KP, Ramanathan R. Digital Signal and Image processing- The Sparse way. Isa Publishers. Elsevier 2012; pp. 408–416. ISBN: 978-93-81269-49-7.
42. Blomgren P, Chan TF. Color TV: Total variation methods for restoration of vector valued images. IEEE Transactions on Image Processing 2002; 7(3): 304–309. DOI 10.1109/83.661180.
43. Duran J, Coll B, Sbert C. Chambolle's Projection Algorithm for Total Variation Denoising. Image Processing On Line 2013; 3:311–331.
44. Rudin LI, Osher S, Fatemi E. Nonlinear total variation based noise removal algorithms. Physica D 1992; 60: 259–268.
45. Caselles V. Total variation based image denoising and restoration. Proc. Intern. Congr. Math. 2006; 03: 1453–1472.
46. Daugman JG. Uncertainity relation for resolution in space, Spatial frequency, and orientation optimized by two-dimensional visual cortical filters. J. Opt. Soc. Am. A 1985; 2(7): 1160–1169.
47. Gabor D. Theory of communication. J. of IEE Japan 1946; 93(26): 429–457.
48. Kaur A, Jindal G. Texture Based Image segmentation using gabor filters. Int. J. Engg. Sc. and Adv. Tech. 2012; 2(3): 687–689.
49. Gupta L, Dixit S. Analysis of Abnormalities in MRI Images of Brain. Int. J. Emer. Res. Manag. Tech. (IJEMRT) 2015; 4(2): 14–18.
50. Gupta P, Pahwa K. Visual Quality Improvement of Medical Images using Pixel reconstruction followed by gabor enhancement technique. Int. J. of Signal Processing, Image Processing and Pattern Recognition 2014; 7(6): 297–302.
51. Veni S, Narayanankutty KA. Image enhancement of medical images using gabor filter bank on hexagonal sampled grids. Int. Schol. Sci. Res. & Inn. 2010; 4(5): 648–653.
52. Bhattacharya D, Devi J, Bhattacherjee P. Brain image segmentation technique using Gabor filter parameter. Am. J. Engg. Res. 2013; 2(9): 127–132.